

# NONLINEAR EFFECTS ON CONFOCAL-BEAM RADIATION-FORCE IMAGING

Alexia Giannoula, Dimitrios Hatzinakos, and Richard S. C. Cobbold

The Edward S. Rogers Sr. Department of Electrical and Computer Engineering,  
University of Toronto, Toronto, Ontario M5S 3G4  
e-mail: alexia@comm.utoronto.ca

## ABSTRACT

The dynamic acoustic radiation force produced by two confocal ultrasound beams, can be used for imaging the acoustic properties of tissue. In this paper we investigate how nonlinear propagation in an attenuating medium can affect image quality. Specifically, the effects of the second harmonic on the image formation process are studied, by means of the system point-spread-function (PSF). Incorporation of tissue nonlinearities in the model and extraction of higher-harmonic information, indicates that a more localized radiation force distribution and reduced sidelobe effects can be achieved and this could improve image resolution.

## 1. INTRODUCTION

When a continuous ultrasound wave propagates in an attenuating medium, both an oscillating and a steady-state force component are produced. The latter is called the radiation force. By modulating the ultrasound wave (typically at quite low frequencies) the radiation force varies in time and the resulting force is usually referred to as a dynamic radiation force. Because relatively high-frequency ultrasound can penetrate and be focused in tissue, it is possible to generate a highly localized radiation force that can be used as a probe, to image the elastic properties of tissue for diagnostic applications [1]-[3].

Fatemi and Greenleaf introduced a new ultrasound imaging modality, which they called vibro-acoustography [2]. They showed that it is potentially capable of producing high-resolution maps of the mechanical properties of an object, that vibrates in response to a highly localized dynamic radiation force. This method belongs to a general class of techniques, commonly referred to as elasticity imaging. Measurement of the vibrations could be useful for assessing tissue stiffness and potentially aid to diagnose the presence of abnormal structures within body tissue. Fig. 1 illustrates the method setup. The transducer consists of two confocal CW ultrasound sources excited at slightly different frequencies,

This work was supported by the Natural Sciences & Engineering Research Council of Canada (NSERC)

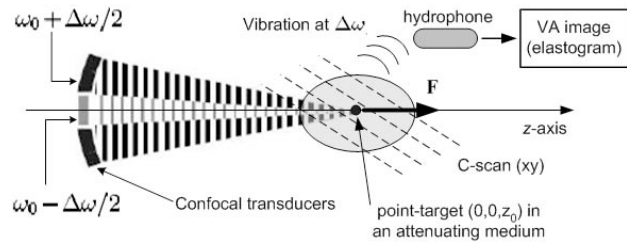


Figure 1: Radiation-force imaging. By scanning the focal point over the  $xy$ -plane an image of the elasticity distribution can be obtained.

resulting in a dynamic radiation force at the common focal point.

In most elasticity imaging techniques, the assumption has been made that ultrasound beams propagate in a linear manner. However, for high-intensity focused ultrasound, such as that needed to produce a significant radiation force, nonlinear effects can become important, particularly the generation of higher harmonics [4]. By extracting harmonic information, a smaller and less distributed effective sample volume is generated, leading to clutter suppression, reduced image artifacts (less noise and blur) and likely improved resolution.

Specifically in vibro-acoustography, the case of linear propagation of ultrasound in an ideal fluid has been treated so far. In that formulation, if no target exists along the wave path, then there is no net radiation force in the fluid [5]. However, this is not true for dissipative (lossy) fluids. When we deal with attenuating media, where viscous losses occur, the radiation force is nonzero even in the absence of any target object. In fact, as shown in [6], viscosity plays an important role in the assessment of tissue elasticity.

The dynamic acoustic radiation force, produced by two confocal ultrasound beams under nonlinear propagation in tissue, is investigated in this paper. Based on the nonlinear computational model of [7], the dynamic force is modelled for the  $n$ -th harmonic frequency ( $n = 1, 2$ ) and the image formation process is studied through the system point-spread-function (PSF). Incorporating tissue nonlinearities in the propagation model, could improve resolution of vibro-acoustic images.

## 2. NONLINEAR SYSTEM MODEL

In this section, the dynamic radiation force exerted on a point target (particle) of an infinite isotropic, homogeneous and attenuating medium is considered. Using a suitably modulated focused ultrasound beam that propagates in an attenuating medium, it is possible to create an arbitrary volume force distribution in the focal zone. It can be shown to be given by [8]:

$$\mathbf{F}_n(\mathbf{r}, t) = \frac{2\alpha_n \mathbf{I}_n(\mathbf{r}, t)}{c}, \quad n = 1, 2, \dots \quad (1)$$

where  $c$  is the speed of sound in the medium,  $nf_0$  denotes the  $n$ -th harmonic frequency ( $f_0$  is the fundamental frequency) and  $\mathbf{I}_n(\mathbf{r}, t)$  is the corresponding acoustic intensity vector. A power-law frequency dependence for the attenuation coefficient has been assumed. For the  $n$ -th harmonic wave it is given by  $a_n(f) = a_0(f)^b$ , where  $b$  is typically close to unity in tissue. In vibro-acoustography, we are only interested in the time-varying (dynamic) component of the incident intensity vector.

To achieve a localized dynamic (oscillatory) radiation stress field, two intersecting continuous-wave (CW) beams can be used. In the intersection zone, a modulated ultrasound field is produced. Specifically, we assume two coaxial confocal CW ultrasound beams  $a$  and  $b$  excited at frequencies  $\omega_a = \omega_0 - \Delta\omega/2$  and  $\omega_b = \omega_0 + \Delta\omega/2$ , where  $\omega_0$  and  $\Delta\omega$  are the center and modulating frequencies, respectively, with  $\Delta\omega \ll \omega_0$  (see Fig. 1). The beams are taken to propagate in the  $z$ -direction and the common focal point  $\mathbf{r}_0$  to be located at  $(0, 0, z_0)$ . In the linear-propagation case, the resultant velocity potential at the region of intersection can be written, by using the principle of superposition, as follows:

$$\phi(\mathbf{r}, t) = \phi_a(\mathbf{r})e^{j\omega_a t} + \phi_b(\mathbf{r})e^{j\omega_b t} \quad (2)$$

where  $\phi_a(\mathbf{r})$  and  $\phi_b(\mathbf{r})$  are the complex amplitude functions of the ultrasonic beams (phase information has been ignored for the sake of simplicity).

It can be shown that the intensity vector and consequently, the radiation force vector of equation (1), has a time-varying (harmonic) component at the difference frequency  $\Delta\omega$ . This can be described by:

$$\mathbf{I}_n^{(d)}(\mathbf{r}, t) = \frac{1}{2} \text{Re}\{[p_{nb}(\mathbf{r})\mathbf{v}_{na}^*(\mathbf{r}) + p_{na}(\mathbf{r})\mathbf{v}_{nb}^*(\mathbf{r})]e^{jn\Delta\omega t}\} \quad (3)$$

where  $*$  denotes the complex conjugate. For  $n = 1$ , the pressure amplitudes  $p_{1a}$ ,  $p_{1b}$  and velocity amplitudes  $v_{1a}$ ,  $v_{1b}$ , correspond to the two beams  $\omega_a$  and  $\omega_b$ , respectively.

If nonlinear propagation occurs, the resultant intensity field at the region of interference will contain terms not only at the frequencies  $\omega_a$  and  $\omega_b$ , but also ‘‘combination tones’’, with frequencies  $n_1\omega_a \pm n_2\omega_b$  (where  $n_1, n_2$  are

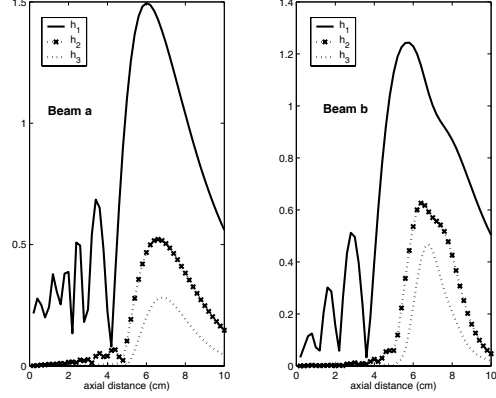


Figure 2: Axial velocity profiles up to third-harmonic ( $n = 1, 2, 3$ ) for both beams.

positive integers) [4]. However, for the purpose of vibro-acoustography, all high-frequency terms can be neglected, as they do not fall within the low acoustic frequency range. If we restrict our attention to the case of  $n_1=n_2=n=2$ , i.e. up to second-harmonic generation for each confocal beam, only two low-frequency (dynamic) components of the resultant intensity vector can be extracted: (a) a component at the beat frequency  $\Delta\omega = \omega_b - \omega_a$ , arising from the interference of the two fundamental waves, as described in equation (3) for  $n = 1$  and (b) another low-frequency term at twice the previous frequency, i.e., at an angular frequency of  $2(\omega_b - \omega_a)$ , arising from the interference of the two second-harmonic signals. In the latter case, the dynamic (low-frequency) intensity vector can be described also by the above equation, if we set  $n = 2$ .

Based on equation (1), the dynamic radiation force corresponding to the  $n$ -th harmonic, is described by:

$$\mathbf{F}_n^{(d)}(\mathbf{r}, t) = \frac{2a_0[n(f_a + f_b)]^b \mathbf{I}_n^{(d)}(\mathbf{r}, t)}{c}, \quad n = 1, 2, \dots \quad (4)$$

where  $\mathbf{I}_n^{(d)}(\mathbf{r}, t)$  is given by equation (3). The attenuation factor is shown to be affected by the sum of the incident harmonic frequencies  $nf_a$  and  $nf_b$ . It should be noted, that the second-order field resulting from the nonlinear interaction of the two primary beams (that would contribute another low-frequency term  $\Delta\omega$ ) [4], has not been taken into account.

The dynamic radiation force described above, causes tissue in the focal zone to vibrate at the difference frequency (see Fig. 1). In response, the zone emits low-frequency longitudinal waves, known as *acoustic emission*, whose amplitudes depend on the radiation force and the elastic properties of the medium [2]. For the nonlinear-propagation case, the received acoustic emission signal can be filtered at multiples of the difference frequency, i.e. at  $n\Delta\omega$  ( $n = 1, 2, \dots$ ), thereby producing the fundamental and harmonic elastography images.

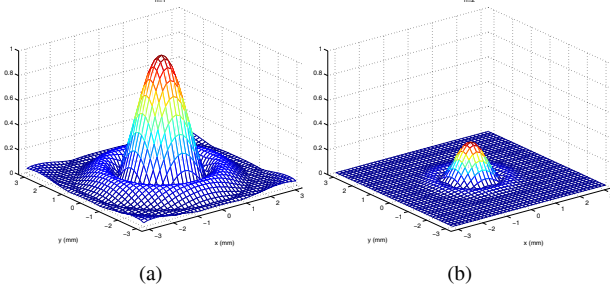


Figure 3: Spatial pattern of the normalized radiation force at the focal plane ( $z = 7$  cm) for (a) the fundamental ( $\Delta\omega$ ) and (b) the second harmonic ( $2\Delta\omega$ ).

### 3. IMAGE FORMATION

To produce an image in vibro-acoustography, the region of interest is scanned either on the  $xz$ -plane ( $B$ -scan, parallel view) or the  $xy$ -plane ( $C$ -scan, transverse view) and the amplitude of the acoustic emission, recorded at a specific focal point of the plane, is assigned to the corresponding pixel of the image output (see Fig. 1). Often, the performance of an imaging system is characterized in terms of its point-spread-function (PSF), which is the image produced by a point-target and describes the degree of blurring of the point-target. To determine the system PSF both for the fundamental and the second harmonic, we consider a unit point target  $\xi(\mathbf{r}_1) = \delta^3(\mathbf{r} - \mathbf{r}_1)$  and we assume that for a fixed focal point  $\mathbf{r}_0$  on the  $xy$ -plane ( $C$ -scan), the object can vary its position  $\mathbf{r}_1$  in the neighborhood of  $\mathbf{r}_0$ . This neighborhood is assumed to be small enough, such that the medium transfer function (which describes the medium characteristics and boundary conditions) remains unchanged.

It is convenient to define the normalized PSF as the normalized response of a unit point-target to the dynamic radiation force of equation (4), i.e.:

$$h_n(\mathbf{r}_1|\mathbf{r}_0) = \frac{P_n^{(d)}(\mathbf{r}_1|\mathbf{r}_0)}{P_n^{(d)}(\mathbf{r}_0|\mathbf{r}_0)} = \frac{\mathbf{F}_n^{(d)}(\mathbf{r}_1|\mathbf{r}_0)}{\mathbf{F}_n^{(d)}(\mathbf{r}_0|\mathbf{r}_0)}, \quad n = 1, 2 \quad (5)$$

where  $P_n^{(d)}$  ( $n = 1, 2$ ) is the acoustic emission field at the difference frequencies  $\Delta\omega$  and  $2\Delta\omega$ , for the fundamental and the second harmonic, respectively. An inherent assumption of equation (4), is that the emitted field can be accurately measured by the hydrophone and as a result, the PSF is spatially shift-variant. Moreover, the radiation force has been defined in the 3-D space. However, only its axial component (parallel to the beam) will be considered in our simulations, as it contributes the most to the formation of the total force.

By convolving the function of a given object with the point-spread-functions described above in a piece-wise shift-invariant manner, two images can be formed, corresponding to  $n = 1$  and  $n = 2$ . It is therefore important to reliably determine  $h_1(\mathbf{r}_1|\mathbf{r}_0)$  and  $h_2(\mathbf{r}_1|\mathbf{r}_0)$  from equation (5), as this

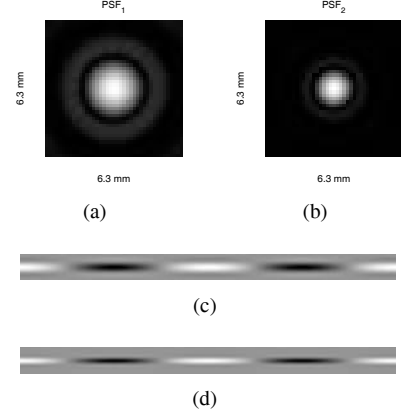


Figure 4: Simulated PSF amplitudes on the focal plane for (a) the fundamental and (b) the second harmonic. Spatiotemporal variations of the dynamic forces on the focal plane over 2 periods of the beat frequencies: (c)  $T_1 = 1/\Delta f$  (fundamental period) and (d)  $T_2 = 1/(2\Delta f)$  (second-harmonic period). Vertical axis: 6.3mm lateral distance, horizontal axis: time.

would enable us to apply an inverse process (deconvolution) to each harmonic image and obtain deblurred estimates of the true scanned object, e.g. similarly to the method proposed in [9] for conventional B-mode ultrasound images. The second-harmonic signal is known to have better resolution and lower sidelobes compared to the fundamental, however its amplitude is lower, leading to lower signal-to-noise-ratio (SNR). Therefore, as noted in the above work, a subsequent fusion of the deblurred harmonic images could result in a single image output of improved resolution.

Finally, it should be noted that when we deal with viscous (dissipative) fluids, except for the acoustic emission signal, shear waves will also arise in response to the radiation force that will propagate away from the beam axis. Approximate expressions of the tissue displacement fields, known as the elastodynamic Green's functions, have been derived for viscoelastic media [6]. However, in our analysis so far, we have ignored the effects of shear-wave propagation on the image formation process. A more thorough description of the underlying physics behind vibro-acoustic image synthesis, will be presented in a subsequent paper.

### 4. SIMULATION RESULTS

Two simple coaxial concave radiation sources were considered, with radii of 1.5 cm for beam- $a$  and 1.68 cm, 2.2 cm for the inner and outer rings of beam- $b$ , respectively, a common focal depth of 7.0 cm and source pressure amplitude of 372 kPa. The sources were assumed to be excited at frequencies  $f_o - \Delta f/2$  and  $f_o + \Delta f/2$ , where  $f_o = 1.5$  MHz and  $\Delta f = 10$  kHz. The propagating medium was taken to have: speed of sound  $c = 1550$  m/s, a density of  $1050$  kg/m<sup>3</sup>, a nonlinearity coefficient of 5,  $b = 1.1$  and

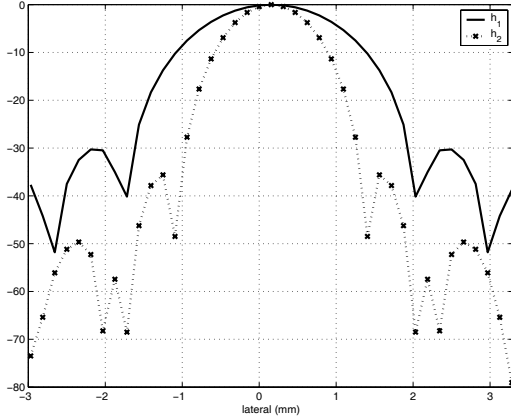


Figure 5: Amplitude of the normalized (steady-state) PSFs for the fundamental and the second harmonic on the focal plane (logarithmic scale).

$\alpha_0 = 0.3 \text{ dB}/(\text{cm MHz}^{1.1})$ . In order to calculate the pressure and velocity fields generated by the transducers, i.e.,  $p_{na}, p_{nb}$  and  $v_{na}, v_{nb}$  ( $n = 1, 2, \dots$ ), we made use of a 2<sup>nd</sup>-order operator-splitting nonlinear model described by Zemp *et al.* [7]. This enabled the harmonic field distribution to be calculated up to  $n = 3$  with reasonable accuracy.

Figure 2 shows the axial velocity profiles of the first three harmonics for beam-*a* (left) and beam-*b* (right). Fifty propagation planes were used to capture the axial variations of the harmonics. Closer to the transducer, the approximations used in the nonlinear propagation algorithm cause errors in the calculated velocity profiles. The third harmonic ( $n = 3$ ) will be ignored in our subsequent simulations.

As described in Section 2, at the focal plane ( $z = 7 \text{ cm}$ ) where the beams intersect, two dynamic components of the radiation force arise at  $\Delta\omega$  and  $2\Delta\omega$ , due to the interference of the fundamental ( $n = 1$ ) and the second-harmonic ( $n = 2$ ) waves, respectively. The spatial patterns of the dynamic radiation force at a given time instant, can be seen in Fig. 3(a) for  $n = 1$  and Fig. 3(b) for  $n = 2$ , based on equations (3), (4) and the calculated pressure and velocity fields. The forces have been normalized with respect to the maximum of the fundamental. The second harmonic is 29.7% of the fundamental at the focal point. This was found, subsequently, to result in an acoustic emission signal  $P_2^{(d)}$  of amplitude approximately equal to 30.4% of the amplitude of  $P_1^{(d)}$ .

The two point-spread-functions (PSFs) corresponding to  $\Delta\omega$  and  $2\Delta\omega$ , were also simulated based on equation (5) and their amplitudes can be seen in Fig. 4(a) and 4(b), at a 6.3mm x 6.3mm transverse view of the focal plane. Figs. 4(c)-(d) show the spatiotemporal distribution of the dynamic force over two periods  $2T_1$  and  $2T_2$  of the corresponding beat frequencies.

The lateral profiles of the normalized PSFs are shown in Fig. 5 in a logarithmic scale. Visual inspection of the above

figures, demonstrates that  $h_2$  has a narrower mainlobe and lower sidelobes than  $h_1$ , that can provide sharper focusing and reduced image artifacts. Specifically, the spatial resolution of  $h_1$  in the lateral direction (defined by the diameter of the mainlobe at  $-6 \text{ dB}$  from its peak) is approximately 1.9 mm and its first sidelobe is under  $-30 \text{ dB}$ . For  $n = 2$ , the lateral resolution of  $h_2$  is calculated to be approximately 1.1 mm, i.e. an improve of almost 42% is achieved, while its first sidelobe is under  $-35.5 \text{ dB}$ .

## 5. CONCLUSIONS

Modelling of the dynamic radiation force produced by two intersecting nonlinear ultrasound beams in tissue, has been presented for vibro-acoustic imaging. The effects of the second harmonic were also studied on the image formation process. To the best of our knowledge, there has been no previous publication that accounts for the effects of harmonic generation in an attenuating medium for vibro-acoustography applications. Incorporation of tissue nonlinearities in the propagation model, was shown to provide a more localized radiation force field and reduced sidelobe effects on the system PSF, which can be used to improve vibro-acoustic image resolution.

## 6. REFERENCES

- [1] A. P. Sarvazyan, O. V. Rudenko, D. Scott, J. Swanson, B. Fowlkes, and S. Y. Emelianov, "Shear wave elasticity imaging: a new ultrasonic technology of medical diagnostics," *Ultrasound in Medicine and Biology*, vol. 24, pp. 1419–1435, 1998.
- [2] M. Fatemi and J.F. Greenleaf, "Ultrasound-stimulated vibro-acoustic spectrography," *Science*, vol. 280, pp. 82–85, April 1998.
- [3] K. Nightingale, M. Palmeri, K. Frinkley, A. Sharma, Z. Liang, and G. Trahey, "Ultrasonic imaging of the mechanical properties of tissues using localized, transient acoustic radiation force," in *Proc. of Int. Conf on Acoustics, Speech, and Signal Processing (ICASSP)*, 2005, vol. 5, pp. 981–984.
- [4] M. F. Hamilton and D. T. Blackstock, *Nonlinear Acoustics*, Academic Press, London, UK, 1998.
- [5] K. Beissner, "The acoustic radiation force in lossless fluids in eulerian and lagrangian coordinates," *J. Acoust. Soc. Am.*, vol. 103, pp. 2321–2332, 1998.
- [6] J. Bercoff, M. Tanter, M. Muller, and M. Fink, "The role of viscosity in the impulse diffraction field of elastic waves induced by the acoustic radiation force," *IEEE Trans. on Ultrasonics, Ferroelectrics and Frequency Control*, vol. 51, pp. 1523–1536, 2004.
- [7] R. J. Zemp, J. Tavakkoli, and R. S. C. Cobbold, "Modeling of nonlinear ultrasound propagation in tissue from array transducers," *J. Acoust. Soc. Am.*, vol. 113, pp. 139–152, 2003.
- [8] G. R. Torr, "The acoustic radiation force," *Am. J. Phys.*, vol. 52, pp. 402–408, 1984.
- [9] T. Taxt and R. Jirik, "Superresolution of ultrasound images using the first and second harmonic signal," *IEEE Trans. on Ultrasonics, Ferroelectrics and Frequency Control*, vol. 51, pp. 163–174, 2004.